Nonlinear Numerical Analysis of Axisymmetrically Loaded Arbitrary Shells of Revolution

PHILIP MASON,* ROBERT RUNG,* JACOB ROSENBAUM,† AND REIN EBRUS‡
Grumman Aircraft Engineering Corporation, Bethpage, Long Island, N. Y.

The nonlinear interaction between the meridional stress resultant and rotation is significant in discontinuity regions of highly strained, thin-shell structures. The nonlinear equilibrium equations may be linearized for any given axisymmetric-load condition by inserting the meridional stress resultant, obtained from membrane analysis, where it appears in product terms. Forward integration is used to solve the set of linear differential equations that is derived from the linear strain-displacement relations and the linearized equilibrium equations. By introducing artificial boundaries within the shell, the extent of integration is limited to conform with available numerical techniques. Influence coefficients for segments are computed, and standard methods of matrix structural analysis are used to obtain stress resultants and displacements at the segment interfaces. These are used as initial values for a final numerical integration to determine stresses and displacements throughout the shell. The differences between stresses calculated by means of linear and nonlinear equations are represented graphically from the results of the analysis of a typical pressure vessel support joint. The well-known reduction of peak stresses in the vessel wall is verified, but the bending stress in the support skirt is greater with the nonlinear analysis.

Nomenclature

$N_\phi, N_\theta, Q_\phi, M_\phi, M_\theta$	= stress resultants (Fig. 2.)
$\bar{N}_\phi$	= a priori value of meridional stress resultant
$Q_\phi{}^*$	= nonlinear transverse shear-stress resultant
M	= moment at boundary of segment, measured in over-all coordinate system
F_R, F_Z	= forces in radial and axial directions, measured in over-all coordinate system
f	= distributed load, psi
E	= Young's modulus
h	= thickness
r_0, r_1, r_2	= radii defined in Fig. 2
v, w	= displacements in meridional and normal directions, respectively
$\omega_\theta, \Delta_R, \Delta_Z$	= rotation and displacements at ϕ, measured in over-all coordinate system
$\epsilon_\theta, \epsilon_\phi$	= strains in θ and ϕ direction, respectively
k_θ, k_ϕ	= change in curvature in θ and ϕ directions, respectively
$\sigma_\theta, \sigma_\phi$	= stresses in θ and ϕ directions, respectively
σ_e	= Huber-Von Mises-Hencky effective stress
ν	= Poisson's ratio
β^4	= $[3(1 - \nu^2)/r_0{}^2h^2]$ for cylinder
γ	= $[3(1 - \nu^2]^{1/2}(N_\phi r_0/Eh^2)$ for cylinder
Λ	= $(1 + \gamma)^{1/2}\beta z$ = segment-length parameter

Introduction

CONVENTIONAL linear stress analysis of thin-shell pressure vessels for space application is not wholly satisfactory for many design configurations. Nonlinear effects may be significant in discontinuity regions of a shell structure (e.g., local thickening or multiple intersections). Critical weight considerations of current aerospace structures require more exact analysis methods to achieve optimum design. This paper presents a practical method for nonlinear analysis of axisymmetrically loaded arbitrary shells of revolution.

The analysis is based on Kempner's[1] nonlinear generalization of the first-order linear-shell equilibrium equations and boundary conditions given by Reissner.[2] The shell equilibrium equations are generalized by including nonlinear terms, which contain the product of the meridional stress resultant and the change in curvature. Boundary conditions are modified also to allow for nonlinear effects. The corresponding nonlinear terms (squares of rotation) in the strain-displacement relations are negligible for many applications and are not included.

These general equations are used to form a set of six simultaneous nonlinear differential equations in six variables; these are three displacements and three effective boundary-stress resultants. The nonlinear terms always include the meridional stress resultant; hence they may be linearized for a particular loading by replacing the "unknown" meridional stress resultant with the distribution obtained from a linear analysis.

Within a finite region, the solution for six given boundary conditions and distributed load may be obtained by combining seven separate solutions (corresponding to two edge shears, two edge moments, two applied axial-edge loads, and the given surface loading). Assuming arbitrary values of the boundary forces and displacements at one edge of a finite region, the equations may be integrated numerically as an initial value problem to the other boundary. Repeating the integration with six different initial conditions and the distributed load condition provides a set of seven solutions. These solutions then may be combined linearly to satisfy the given surface loading and boundary conditions.

Because of the exponentially decaying behavior of the stresses and displacements, the length of the region that can be analyzed in the manner described is limited by numerical difficulties of small differences of large numbers.[3,8,9] To extend this limit, artificial boundaries are introduced within the region of interest. The procedure then may be applied between these boundaries to obtain influence coefficients for each segment from the initial and terminal values of the six solutions for the applied edge forces. Matrix techniques are used to solve for stress resultants and displacements between adjacent segments. These forces and displacements are used then as initial values for a final integration through the segments to obtain the numerical solution.

A comparison of the present method with an analytic solution[5] for a cylinder subjected simultaneously to a uniform

Presented as Preprint 64-439 at the AIAA Annual Meeting, Washington, D. C., June 29–July 2, 1964; revision received March 23, 1964.

* Structural Methods Engineer.
† Structural Methods Engineer. Associate Member AIAA.
‡ Computer Analyst.

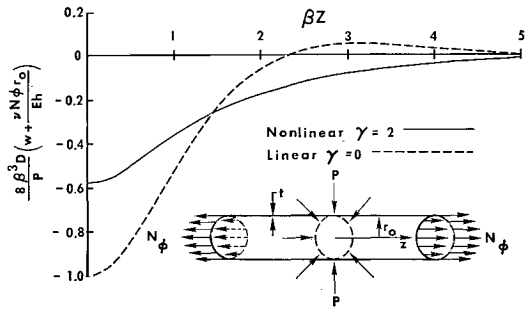

Fig. 1 Nondimensional radial displacement of line-loaded cylinder.

radial-line load P and axial tension N_ϕ has been made. Figure 1 shows the linear and nonlinear results. The analytic and numerical results are indistinguishable.

Nonlinear Equations

The three equations of equilibrium[4] for an axisymmetrically loaded shell of revolution are, in accordance with Fig. 2,

$$\left.\begin{aligned} \Sigma F_\varphi = 0 \qquad & (d/d\varphi)(N_\varphi r_0) - N_\theta r_1 \cos\varphi - r_0 Q_\varphi = \\ & -r_1 r_0 (f_\varphi + f_\varphi{}^*) \\ \Sigma F_\zeta = 0 \qquad & (d/d\varphi)(Q_\varphi r_0) + N_\varphi r_0 + N_\theta r_1 \sin\varphi = \\ & -r_1 r_0 (f_\zeta + f_\zeta{}^*) \\ \Sigma M_\varphi = 0 \qquad & (d/d\varphi)(M_\varphi r_0) - M_\theta r_1 \cos\varphi - \\ & Q_\varphi r_1 r_0 = 0 \end{aligned}\right\} \tag{1}$$

where

$$f_\varphi{}^* = -\bar{N}_\varphi \omega_\theta / r_1$$
$$f_\zeta{}^* = (1/r_0 r_1)(d/d\varphi)(r_0 \bar{N}_\varphi \omega_\theta) \tag{2}$$

The nonlinear terms $f_\varphi{}^*$ and $f_\zeta{}^*$ result from the action of the stress resultants on the deformed shell. Figure 3 shows the original and deformed states of a shell element that has undergone a rotation ω_θ. Thus, the stress resultant N_φ has components normal to the undeformed shell surface equal to $\{N_\varphi \omega_\theta\}$ and $\{N_\varphi \omega_\theta + (d/d\phi)(N_\varphi \omega_\theta) d\phi\}$ at the edges of the element. These components are resolved into the local ϕ and ζ coordinates to obtain

$$dF_\varphi{}^* = -N_\varphi \omega_\theta r_0 (d\theta d\varphi/2) - \{N_\varphi \omega_\theta + (d/d\varphi)(N_\varphi \omega_\theta) d\varphi\} \times [r_0 + (dr_0/d\varphi) d\varphi](d\theta d\varphi/2) = -N_\varphi \omega_\theta r_0 d\theta d\varphi$$

$$dF_\zeta{}^* = -N_\varphi \omega_\theta r_0 d\theta + \{N_\varphi \omega_\theta + (d/d\varphi)(N_\varphi \omega_\theta) d\varphi\} \times [r_0 + (dr_0/d\varphi) d\varphi] d\theta = (d/d\varphi)(N_\varphi \omega_\theta r_0) d\theta d\varphi$$

Dividing by the element area $r_0 r_1 d\theta d\phi$ yields

$$f_\varphi{}^* = dF_\varphi{}^*/dA = -\bar{N}_\varphi \omega_\theta / r_1$$
$$f_\zeta{}^* = dF_\zeta{}^*/dA = (1/r_0 r_1)(d/d\varphi)(\bar{N}_\varphi \omega_\theta r_0)$$

where N_φ is replaced by $\bar{N}_\varphi$, the distribution obtained from a linear or membrane analysis of the given loading, thereby linearizing the differential equations.

By similar reasoning, it may be shown that the product $N_\varphi \omega_\theta$ contributes to the transverse shear

$$Q_\varphi{}^* = Q_\varphi + \bar{N}_\varphi \omega_\theta \tag{3}$$

Substituting $f_\varphi{}^*$, $f_\zeta{}^*$, and $Q_\varphi{}^*$ into Eqs. (1) and using the geometric identity

$$dr_0/d_\varphi = r_1 \cos\varphi$$

leads to the following form for the equations of equilibrium:

$$\left.\begin{aligned} \frac{1}{r_1}\frac{dN_\varphi}{d\varphi} &= +(N_\theta - N_\varphi)\frac{\cos\varphi}{r_0} + \frac{Q_\varphi{}^*}{r_1} - f_\varphi \\ \frac{1}{r_1}\frac{dQ_\varphi{}^*}{d\varphi} &= -Q_\varphi{}^*\frac{\cos\varphi}{r_0} - \frac{N_\varphi}{r_1} - \frac{N_\theta}{r_0}\sin\varphi - f_\zeta \\ \frac{1}{r_1}\frac{dM_\varphi}{d\varphi} &= +(M_\theta - M_\varphi)\frac{\cos\varphi}{r_0} + Q_\varphi{}^* - \bar{N}_\varphi \omega_\theta \end{aligned}\right\} \tag{4}$$

The expressions for the rotation, curvatures, and strains[4] are, in accordance with Fig. 4,

$$\omega_\theta = (1/r_1)[(dw/d\varphi) + v] \tag{5}$$

$$k_\theta = (\omega_\theta/r_0)\cos\varphi \qquad k_\varphi = (1/r_1)(d\omega_\theta/d\varphi) \tag{6}$$

$$\left.\begin{aligned} \epsilon_\theta &= (1/r_0)(v\cos\varphi - w\sin\varphi) - \zeta k_\theta \\ \epsilon_\varphi &= (1/r_1)[(dv/d\varphi) - w] - \zeta k_\varphi \end{aligned}\right\} \tag{7}$$

From Hooke's Law and Eqs. (7), the stresses are

$$\left.\begin{aligned} \sigma_\theta &= \frac{E}{1-\nu^2}\{\epsilon_\theta + \nu\epsilon_\varphi\} = \frac{E}{1-\nu^2}\left\{\frac{v\cos\varphi}{r_0} - \frac{w\sin\varphi}{r_0} + \frac{\nu}{r_1}\frac{dv}{d\varphi} - \frac{\nu w}{r_1} - \zeta(k_\theta + \nu k_\varphi)\right\} \\ \sigma_\varphi &= \frac{E}{1-\nu^2}\{\epsilon_\varphi + \nu\epsilon_\theta\} = \frac{E}{1-\nu^2}\left\{\frac{1}{r_1}\frac{dv}{d\varphi} - \frac{w}{r_1} + \frac{\nu v\cos\varphi}{r_0} - \frac{\nu w\sin\varphi}{r_0} - \zeta(k_\varphi + \nu k_\theta)\right\} \end{aligned}\right\} \tag{8}$$

Substituting the expressions for the stresses into the defini-

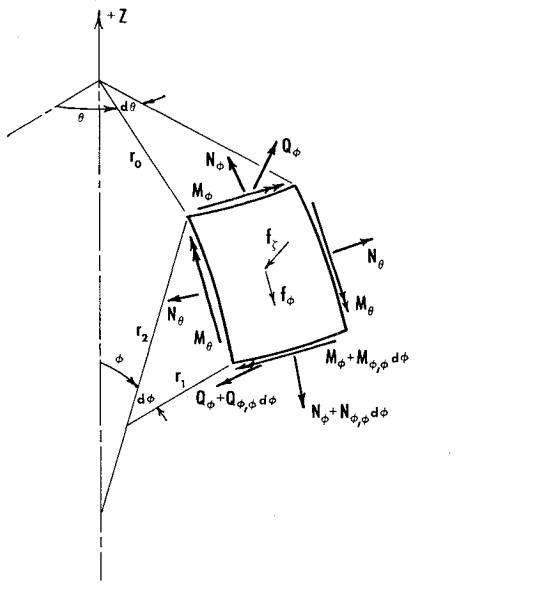

Fig. 2 Shell element.

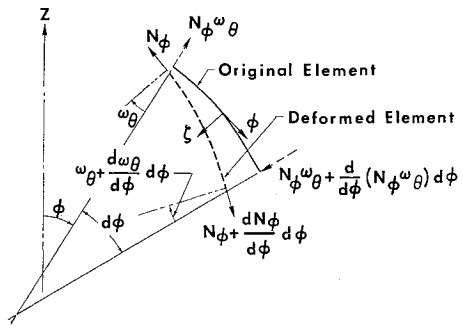

Fig. 3 Nonlinear effects.

tions of the stress resultants yields

$$\left.\begin{aligned}
N_\theta &= \int_{-h/2}^{h/2} \sigma_\theta d\zeta = \\
&\quad \frac{Eh}{1-\nu^2}\left\{\frac{v\cos\varphi}{r_0} - \frac{w\sin\varphi}{r_0} + \frac{\nu}{r_1}\frac{dv}{d\varphi} - \frac{\nu w}{r_1}\right\} \\
N_\varphi &= \int_{-h/2}^{h/2} \sigma_\varphi d\zeta = \\
&\quad \frac{Eh}{1-\nu^2}\left\{\frac{1}{r_1}\frac{dv}{d\varphi} - \frac{w}{r_1} + \frac{\nu v\cos\varphi}{r_0} - \frac{\nu w\sin\varphi}{r_0}\right\} \\
M_\theta &= \int_{-h/2}^{h/2} \sigma_\theta \zeta d\zeta = -D\{k_\theta + \nu k_\varphi\} = \\
&\quad -D\left\{\frac{\omega_\theta\cos\varphi}{r_0} + \frac{\nu}{r_1}\frac{d\omega_\theta}{d\varphi}\right\} \\
M_\varphi &= \int_{-h/2}^{h/2} \sigma_\varphi \zeta d\zeta = -D\{k_\varphi + \nu k_\theta\} = \\
&\quad -D\left\{\frac{1}{r_1}\frac{d\omega_\theta}{d\varphi} + \frac{\nu\omega_\theta\cos\varphi}{r_0}\right\}
\end{aligned}\right\} \quad (9)$$

The desired set of six simultaneous first-order differential equations and three algebraic auxiliary equations are obtained from Eqs. (3–5 and 9):

$$\frac{1}{r_1}\frac{dN_\varphi}{d\varphi} = (N_\theta - N_\varphi)\frac{\cos\varphi}{r_0} + \frac{Q_\varphi^*}{r_1} - f_\varphi \quad (10a)$$

$$\frac{1}{r_1}\frac{dQ_\varphi^*}{d\varphi} = -Q_\varphi^*\frac{\cos\varphi}{r_0} - \frac{N_\varphi}{r_1} - N_\theta\frac{\sin\varphi}{r_0} - f_\zeta \quad (10b)$$

$$\frac{1}{r_1}\frac{dM_\varphi}{d\varphi} = (M_\theta - M_\varphi)\frac{\cos\varphi}{r_0} + Q_\varphi^* - \bar{N}_\varphi\omega_\theta \quad (10c)$$

$$\frac{1}{r_1}\frac{dv}{d\varphi} = \frac{1}{Eh}(N_\varphi - \nu N_\theta) + \frac{w}{r_1} \quad (10d)$$

$$\frac{1}{r_1}\frac{d\omega_\theta}{d\varphi} = \frac{-12}{Eh^3}(M_\varphi - \nu M_\theta) \quad (10e)$$

$$(1/r_1)(dw/d\varphi) = \omega_\theta - v/r_1 \quad (10f)$$

$$N_\theta = \nu N_\varphi + (Eh/r_0)(v\cos\varphi - w\sin\varphi) \quad (10g)$$

$$M_\theta = \nu M_\varphi - (Eh^3/12r_0)(\omega_\theta\cos\varphi) \quad (10h)$$

$$Q_\varphi = Q_\varphi^* - \bar{N}_\varphi\omega_\theta \quad (10i)$$

Use of this system in calculation is described in the Appendix.

Example

The differences between linear and nonlinear analyses are demonstrated by considering the support joint of a typical skirt-supported titanium pressure vessel subjected to uniform internal pressure of 405 psi (Fig. 5). The structure is idealized with cylinders, a sphere, and an ogival section (Fig. 5). A fictitious "kinematic link" is used at the joint in order to maintain the appropriate kinematic relations between middle surfaces of connected shells. It is apparent that the bending stresses given by any shell theory will be physically inconsistent at such a joint. However, this will have negligible effect on the over-all stress distribution.

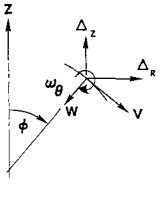

Fig. 4 Displacement sign convention.

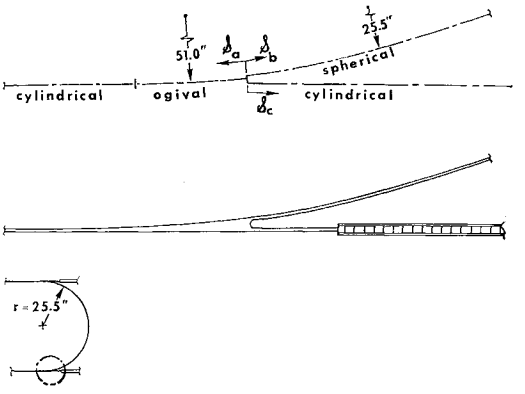

Fig. 5 Typical pressure vessel support joint.

The analysis need not extend farther from the discontinuity than the penetration of the bending behavior. With some experience, the limits of the discontinuity region can be anticipated. Membrane loads $\bar{N}_\phi$, determined by axial equilibrium, are applied at the ends of the idealization. By introducing artificial boundaries within the idealization, the length of each segment is limited to permit accurate forward integration. Figures 6 and 7 present the Huber-Von Mises-Hencky "effective stress"

$$\sigma_e = (\sigma_\theta^2 - \sigma_\theta\sigma_\varphi + \sigma_\varphi^2)^{1/2}$$

for the inside and outside surfaces of the shell. Use of this criterion for design is not recommended; however, it is useful for comparison, since it combines both stress components in a consistent manner characterized by a single number.

The stresses in the thick ogival section are low as compared with those obtained farther from the juncture. The linear results generally are higher than the nonlinear stresses in the pressure-stiffened tank shells. Both asymptotically approach the membrane stress values at greater distances (not shown); the linear from above, the nonlinear from below. In the cylindrical portion of the tank at approximately $\delta_a = 4$ in., the linear stress on the critical outside surface (Fig. 7) is at least 20% greater than the nonlinear value. However, in the skirt, the linear analysis is unconservative, i.e., within 1 in. of the juncture, the linear stresses are at least 30% less than corresponding nonlinear values (Figs. 6 and 7).

The line-loaded cylinder of Fig. 1 and the pressure vessel (Fig. 5) discussed previously demonstrate some typical nonlinear effects. It is not practical to present a detailed parametric discussion of these effects since a refined analysis of this type will lead to a particular geometry for each shell

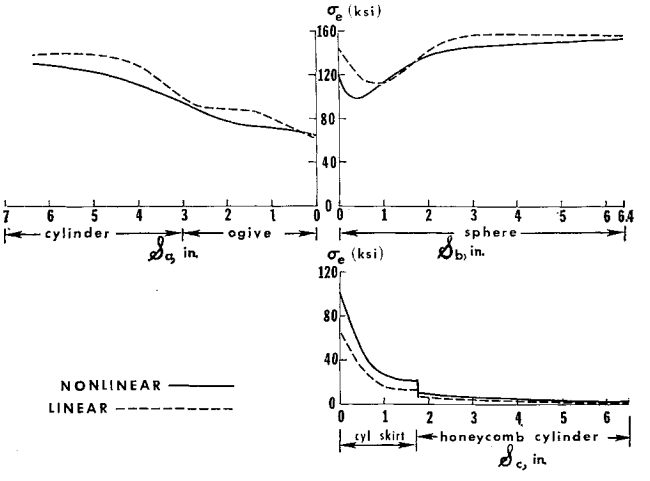

Fig. 6 Effective stress σ_e inside surfaces of pressure vessel.

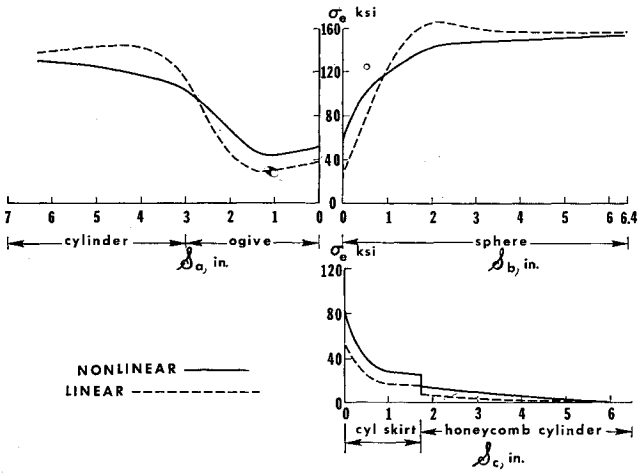

Fig. 7 Effective stress σ_e outside surfaces of pressure vessel.

configuration and load. The distribution of reinforcing thickness at a discontinuity is of paramount importance. (References 5 and 6 give some basic information for constant thickness cylinders and spheres, respectively.)

Significant changes in stress have been found near the bosses in aluminum pressure vessel covers and at multiple intersections where the stress distribution may be affected seriously, often at the expense of one shell. Nonlinear effects are pronounced for highly strained thin shells. For example, in a pressurized cylinder,

$$\gamma = [3(1 - \nu^2)]^{1/2}(N_\varphi r_0/Eh^2) = 2[3(1 - \nu^2)]^{1/2}(\sigma_d{}^2/pE)$$

where σ_d is the design stress, and p is the internal pressure. Thus, high-strength, elastic materials in low-pressure applications are most critical. Further, the size of the vessel is not a factor. For the membrane region of the pressure vessel considered, $\gamma \approx 9$, which is much greater than ($\gamma = 2$) in the simple cylinder. The stresses of the pressure vessel are not affected as dramatically because of the tapered thickness. Typical experimental stress distributions for thin pressure vessels are presented in Ref. 7.

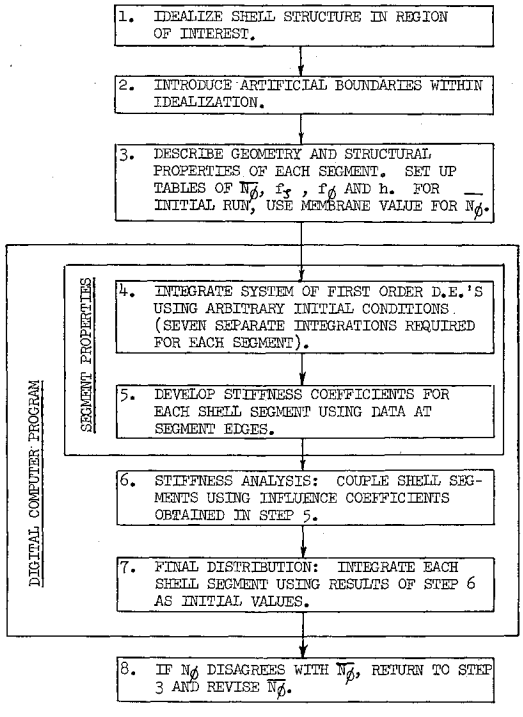

Fig. 8 Outline of analysis.

In a physical sense, the nonlinearities act to stiffen a given shell region, since their effect is to restrict change in curvature. This is demonstrated with edge influence coefficients for spherical shells[6] and has been observed in the stiffness coefficients used in the present method. This phenomenon accounts for the greater penetration of the discontinuity disturbance. For the line-loaded cylinder of Fig. 1, the phenomenon is identical to the beam on an elastic foundation. The nonlinearities add "tie-rod" (opposite of beam-column) effects to the "beam." The deflection under the load is reduced at the expense of greater penetration along the meridian. The same behavior is observed in the pressure vessel, and it is this smaller radial expansion that reduces the hoop stresses σ_θ, thus lowering the effective stress σ_e (Figs. 6 and 7).

Applications

The set of equations [Eqs. (10a–10i)] may be specialized for any desired shell of revolution (such as sphere, ogive, parabola, cylinder, cone, etc.) by inserting the appropriate geometric relationships. The cone may be reduced to a flat plate; in this case, the technique is valid only for a linear analysis. Segments of various types may be combined to form any desired shell. Small segments of cylinders and plates may be used to include support rings in the analysis of the shell. This is convenient and more accurate than the conventional ring idealization.

In addition to branched configurations of the meridian (as in the support joint discussed previously), the method is directly applicable to multiply-connected surfaces such as toroidal shells. This conclusion may be drawn from the analogy to the stiffness analysis of a frame (see Appendix).

Unsymmetric Case

Shells of revolution may be unsymmetrically loaded by lateral loads or by interaction with nonuniform supporting structures. The present technique for axisymmetrically loaded shells may be generalized by using the unsymmetric shell equations.[1] They are cast into eight partial differential equations, which are of second order in the circumferential coordinate θ and of first order in the meridional coordinate ϕ. All of the quantities are expanded by using the Fourier series in the coordinate θ; this reduces the partial differential equations to ordinary differential equations, one set for each harmonic. For the linear theory, each term of the series is uncoupled from the others, and the method parallels the axisymmetric case. The authors have applied this technique successfully for the linear unsymmetric analysis of several thin-shell structures, including some loading conditions of the pressure vessel of Fig. 5. The nonlinear case leads to interaction of all of the harmonics. By considering only a few harmonics (e.g., H), there will be ($8H$) first-order ordinary differential equations to solve simultaneously. Since the stiffness matrix for the linear unsymmetric case is ($4m$) $\times$ ($4m$), where m is the number of joints, the nonlinear case would involve a matrix that is ($4mH$) $\times$ ($4mH$), thus requiring a larger inversion. This approach may be useful for relatively simple cases such as antisymmetric loading.

Shallow Shells

In dealing with shallow shells, two difficulties arise. First, the membrane force $\bar{N}_\phi$ may not be computed accurately by equilibrium considerations since $Q_\phi{}^*$ has a significant effect for small ϕ. Second, the nonlinearity of strain-displacement relations may become significant (as in large-deflection plate theory). The former may be resolved by iteration (Appendix). The latter must be considered as a bound on the capability of the present theory. The theory may be extended and iteration applied to the nonlinear

strain terms by writing $\frac{1}{2}\bar{\omega}_\theta\omega_\theta$, using $\bar{\omega}_\theta$ as the a priori value. For a discussion of the domains of applicability of these nonlinearities, see Refs. 6, 10, and 11.

Appendix

Computational Procedure

The method of analysis will be described by referring to the outline in Fig. 8. The idealized structure is divided into segments of an approximately equal length parameter

$$\Lambda = (1 + \gamma)^{1/2}\beta_z$$

Since the differential equations have been linearized, influence coefficients may be obtained conveniently by superposition of appropriate solutions of initial-value problems. The set of six differential equations, plus the three algebraic auxiliary equations [see Eqs. (10a–10i)], which were developed previously, are solved using a conventional forward integration technique. Variable thickness, loading, and $\bar{N}_\phi$ are taken into account by providing a table of h, f_ϕ, f_ζ, and $\bar{N}_\phi$ vs ϕ and interpolating between tabular values. The set of equations is integrated seven times, using the initial conditions shown in Fig. 9. The first six integrations use unit values of $\omega_{\theta i}$, ΔR_i, Δz_i, M_i, F_{Ri}, and F_{zi}, respectively. During these six integrations, the applied loads f_ϕ and f_ζ are set equal to zero. For the seventh integration, the given distributions of f_ϕ and f_ζ are used, with the initial displacements and stress resultants set equal to zero. The values of the stress resultants and displacements (in shell coordinates) at the jth end of the segment are recorded in the matrices $[X]$ and $[Y]$ for all of the integrations (Fig. 9). Thus

$$\{f_j\} = \underset{3\times3}{\left[\begin{array}{c|c|c}[X_1] & [X_2] & [X_3]\end{array}\right]}\begin{Bmatrix}\Delta_i \\ \overline{F_i} \\ \overline{L}\end{Bmatrix} \tag{A1}$$

$$\{\delta_j\} = \underset{3\times3}{\left[\begin{array}{c|c|c}[Y_1] & [Y_2] & [Y_3]\end{array}\right]}\begin{Bmatrix}\Delta_i \\ \overline{F_i} \\ \overline{L}\end{Bmatrix} \tag{A2}$$

where $\{L\}$ is a dimensionless load factor, and $\{f_j\}$, $\{\delta_j\}$, $\{\Delta_i\}$, and $\{F_i\}$ are defined in Fig. 9.

The forces and displacements are rotated from the local-shell coordinate system to the over-all coordinate system by matrices $[A]$ and $[B]$, respectively. Thus

$$\{F_j\} = \begin{Bmatrix}M_j \\ F_{Rj} \\ F_{Zj}\end{Bmatrix} = \left[\begin{array}{c|c|c} 0 & 0 & -1 \\ \cos\varphi_j & -\sin\varphi_j & 0 \\ -\sin\varphi_j & -\cos\varphi_j & 0 \end{array}\right]\begin{Bmatrix}N_{\varphi j} \\ Q_{\varphi j}^* \\ M_{\varphi j}\end{Bmatrix} = \underset{3\times3}{[A]}\{f_j\} \tag{A3}$$

$$\{\Delta_j\} = \begin{Bmatrix}\omega_j \\ \Delta_{Rj} \\ \Delta_{Zj}\end{Bmatrix} = \left[\begin{array}{c|c|c} 0 & 0 & +1 \\ \cos\varphi_j & -\sin\varphi_j & 0 \\ -\sin\varphi_j & -\cos\varphi_j & 0 \end{array}\right]\begin{Bmatrix}v_j \\ w_j \\ \omega_j\end{Bmatrix} = \underset{3\times3}{[B]}\{\delta_j\} \tag{A4}$$

Substituting (A1) into (A3) yields

$$\{F_j\} = \underset{3\times3}{[A]}\underset{3\times3}{\left[\begin{array}{c|c|c}[X_1] & [X_2] & [X_3]\end{array}\right]}\begin{Bmatrix}\Delta_i \\ \overline{F_i} \\ \overline{L}\end{Bmatrix} = \underset{3\times3}{\left[\begin{array}{c|c|c}[AX_1] & [AX_2] & [AX_3]\end{array}\right]}\begin{Bmatrix}\Delta_i \\ \overline{F_i} \\ \overline{L}\end{Bmatrix} \tag{A5}$$

Run Number			1	2	3	4	5	6	7
			Δ_i			F_i			Load
			$\omega_i = 1$	$\Delta_{Ri} = 1$	$\Delta_{Zi} = 1$	$M_i = 1$	$F_{Ri} = 1$	$F_{Zi} = 1$	$L = 1$
Initial Conditions	f_i	$N_{\phi i}$	0	0	0	0	$-\cos\phi_i$	$\sin\phi_i$	0
		$Q_{\phi i}^*$				0	$\sin\phi_i$	$\cos\phi_i$	
		$M_{\phi i}$				+1	0	0	
	δ_i	V_i	0	$\cos\phi_i$	$-\sin\phi_i$	0	0	0	0
		W_i	0	$-\sin\phi_i$	$-\cos\phi_i$				
		ω_i	+1	0	0				
Final Conditions	f_j	$N_{\phi j}$	$\leftarrow\left[X_1\right]_{3\times3}\rightarrow$			$\leftarrow\left[X_2\right]_{3\times3}\rightarrow$			$\left[X_3\right]_{3\times1}$
		$Q_{\phi j}^*$							
		$M_{\phi j}$							
	δ_j	V_j	$\leftarrow\left[Y_1\right]_{3\times3}\rightarrow$			$\leftarrow\left[Y_2\right]_{3\times3}\rightarrow$			$\left[Y_3\right]_{3\times1}$
		W_j							
		ω_j							

Fig. 9 Initial and final conditions.

and substituting (A2) into (A4) yields

$$\{\Delta_j\} = \underset{3\times3}{[B]}\underset{3\times3}{\left[\begin{array}{c|c|c}[Y_1] & [Y_2] & [Y_3]\end{array}\right]}\begin{Bmatrix}\Delta_i \\ \overline{F_i} \\ \overline{L}\end{Bmatrix} = \underset{3\times3}{\left[\begin{array}{c|c|c}[BY_1] & [BY_2] & [BY_3]\end{array}\right]}\begin{Bmatrix}\Delta_i \\ \overline{F_i} \\ \overline{L}\end{Bmatrix} \tag{A6}$$

Equations (A5) and (A6) are used to form (A7) and (A8) as follows:

$$\begin{Bmatrix}\Delta_i \\ \Delta_j \\ L\end{Bmatrix} = \left[\begin{array}{c|c|c} I_3 & 0 & 0 \\ \hline [BY_1] & [BY_2] & [BY_3] \\ 3\times3 & 3\times3 & 3\times1 \\ \hline 0 & 0 & I_1 \end{array}\right]\begin{Bmatrix}\Delta_i \\ \overline{F_i} \\ \overline{L}\end{Bmatrix} = \underset{7\times7}{[Z_1]}\begin{Bmatrix}\Delta_i \\ \overline{F_i} \\ \overline{L}\end{Bmatrix} \tag{A7}$$

$$\begin{Bmatrix}F_i \\ F_j\end{Bmatrix} = \left[\begin{array}{c|c|c} 0 & I_3 & 0 \\ \hline [AX_1] & [AX_2] & [AX_3] \\ 3\times3 & 3\times3 & 3\times1 \end{array}\right]\begin{Bmatrix}\Delta_i \\ \overline{F_i} \\ \overline{L}\end{Bmatrix} = \underset{6\times7}{[Z_2]}\begin{Bmatrix}\Delta_i \\ \overline{F_i} \\ \overline{L}\end{Bmatrix} \tag{A8}$$

Inverting (A7) and substituting into (A8) yields

$$\begin{Bmatrix}F_i \\ F_j\end{Bmatrix} = \underset{6\times7\ 7\times7}{[Z_2][Z_1]^{-1}}\begin{Bmatrix}\Delta_i \\ \Delta_j \\ L\end{Bmatrix} = \underset{6\times7}{[W]}\begin{Bmatrix}\Delta_i \\ \Delta_j \\ L\end{Bmatrix} \tag{A9}$$

$\{F_i\}$ and $\{F_j\}$ are the edge forces at the ith and jth ends of the shell on a unit length basis. It is convenient to work with the total forces $\{\hat{F}_i\}$ and $\{\hat{F}_j\}$. Thus

$$\begin{Bmatrix}\hat{F}_i \\ \hat{F}_j\end{Bmatrix} = \left[\begin{array}{ccc|ccc} \alpha_i & & & & & \\ & \alpha_i & & & & \\ & & \alpha_i & & & \\ \hline & & & \alpha_j & & \\ & & & & \alpha_j & \\ & & & & & \alpha_j \end{array}\right]\begin{Bmatrix}F_i \\ F_j\end{Bmatrix} = \underset{6\times6}{[C]}\begin{Bmatrix}F_i \\ F_j\end{Bmatrix} \tag{A10}$$

where

$$\alpha_i = 2\pi r_{0i} \qquad \alpha_j = 2\pi r_{0j}$$

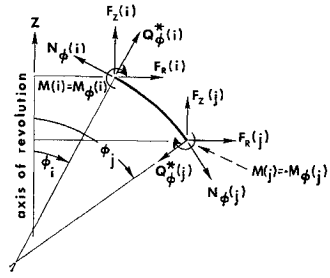

Fig. 10 Force sign convention.

and $[C]$ is a diagonal matrix. Substituting (A9) into (A10) and partitioning yields

$$\underset{6\times 6}{\begin{Bmatrix}\hat{F}_i\\ \hat{F}_j\end{Bmatrix}} = \underset{6\times 6}{[C]}\underset{6\times 7}{[W]}\begin{Bmatrix}\Delta_i\\ \Delta_j\\ L\end{Bmatrix} = \left[\begin{array}{c|c|c}[K] & [G]\end{array}\right]\begin{Bmatrix}\Delta_i\\ \Delta_j\\ \hline L\end{Bmatrix} \tag{A11}$$

The $[K]$ matrix in Eq. (A11) is the stiffness matrix for the shell segment, whereas the $[G]$ matrix is a matrix of fixed end forces, that is, the forces induced at the ends of the segment by distributed loading when the ends are restrained from displacing.

In addition to the $[K]$ and $[G]$ matrices, a matrix that expresses the initial conditions in terms of the displacements at the ith and jth ends of the shell and the applied loading will be required. Referring to Fig. 9,

$$\underset{6\times 7}{\begin{Bmatrix}f_i\\ \delta_i\end{Bmatrix}} = \underset{6\times 7}{[IC]}\begin{Bmatrix}\Delta_i\\ F_i\\ L\end{Bmatrix} \quad \begin{Bmatrix}\Delta_i\\ F_i\\ L\end{Bmatrix} = \underset{7\times 7}{[Z_1]^{-1}}\begin{Bmatrix}\Delta_i\\ \Delta_j\\ L\end{Bmatrix} \tag{A12}$$

Hence

$$\underset{6\times 7}{\begin{Bmatrix}f_i\\ \delta_i\end{Bmatrix}} = \underset{6\times 7}{[IC]}\underset{7\times 7}{[Z_1]^{-1}}\begin{Bmatrix}\Delta_i\\ \Delta_j\\ L\end{Bmatrix} = \underset{6\times 7}{[D]}\begin{Bmatrix}\Delta_i\\ \Delta_j\\ L\end{Bmatrix} \tag{A13}$$

This matrix will be used to set up the initial conditions for the final integration after $\{\Delta_i\}$ and $\{\Delta_j\}$ have been evaluated.

A $[K]$, $[G]$, and $[D]$ matrix is obtained for each shell segment in the idealized structure. For the discussion that follows, it will be convenient to add a subscript n to these matrices to indicate the nth segment.

The total stiffness for the entire structure is the sum of the stiffnesses of the individual segments. Thus

$$\underset{3m\times 3m}{\{\hat{F}_T\}} = \underset{3m\times 3m}{[K_{\text{tot}}]}\{\Delta_T\} \tag{A14}$$

where

$$\underset{3m\times 3m}{[K_{\text{tot}}]} = \sum_{n=1}^{N} \underset{6\times 6}{[K_n]}$$

and N and m are the total number of segments and nodes, respectively. The Σ in Eq. (A14) implies a nonconformal addition; that is, the elements of each $[K_n]$ matrix must be placed in the proper rows and columns of $[K_{\text{tot}}]$.

Displacement boundary conditions are applied by expressing the node displacements in terms of permissible node displacements $\{\Delta_F\}$. Hence

$$\underset{3m\times q}{\{\Delta_T\}} = \underset{3m\times q}{[BC]}\{\Delta_F\} \tag{A15}$$

where q is the number of degrees of freedom. It should be noted that the $[BC]$ matrix will also introduce any "kinematic links" if required, by prescribing the proper relations between displacements. The forces at the free nodes are given by

$$\underset{q\times 3m}{\{\hat{F}_F\}} = \underset{q\times 3m}{[BC]^T}\{\hat{F}_T\} \tag{A16}$$

Hence the stiffness is

$$\underset{q\times 3m}{\{\hat{F}_F\}} = \underset{q\times 3m}{[BC]^T}\ \underset{3m\times 3m}{[K_{\text{tot}}]}\ \underset{3m\times q}{[BC]}\{\Delta_F\} = \underset{q\times q}{[K_{11}]}\{\Delta_F\} \tag{A17}$$

and the flexibility is

$$\underset{q\times q}{\{\Delta_F\}} = \underset{q\times q}{[K_{11}]^{-1}}\{\hat{F}_F\} \tag{A18}$$

The total node loading is composed of two parts; the first, a result of distributed loads acting within a segment and the second, a result of concentrated external forces acting directly on the nodes. If the matrix of external loads is designated as $[L_E]$ then the node loading is given by

$$\underset{q\times 1}{\{\hat{F}_F\}} = \left[\underset{q\times 3m}{-[BC]^T}\underset{3m\times 1}{[G_{\text{tot}}]} + \underset{q\times 1}{[L_E]}\right]\{L\} \tag{A19}$$

where

$$\underset{3m\times 1}{[G_{\text{tot}}]} = \sum_{n=1}^{N} \underset{6\times 1}{[G_n]}$$

Again the Σ implies a nonconformal addition where the elements of $[G_n]$ must be placed in the correct rows of $[G_{\text{tot}}]$. Using Eqs. (A15), (A18), and (A19) yields the node displacements in terms of the applied loading condition. Thus

$$\underset{3m\times 1}{\{\Delta_T\}} = \underset{3m\times q}{[BC]}\underset{q\times q}{[K_{11}]^{-1}}\left[\underset{q\times 3m}{-[BC]^T}\underset{3m\times 1}{[G_{\text{tot}}]} + \underset{q\times 1}{[L_E]}\right]\{L\} = \underset{3m\times 1}{[N]}\{L\} \tag{A20}$$

The displacements and loading conditions for a particular shell segment n that connects nodes i and j are given by

$$\begin{Bmatrix}\Delta_i\\ \Delta_j\\ L\end{Bmatrix} = \begin{bmatrix}[N_i]\\ \hline [N_j]\\ \hline +1\end{bmatrix}\{L\} = \underset{7\times 1}{[P_n]}\{L\} \tag{A21}$$

where the matrices N_i and N_j are the appropriate rows of N. Substituting P_n into D_n gives

$$\underset{6\times 1}{\begin{Bmatrix}f_i\\ \delta_i\end{Bmatrix}} = \underset{6\times 7}{[D_n]}\underset{7\times 1}{[P_n]}\{L\} = \underset{6\times 1}{[E_n]}\{L\} \tag{A22}$$

The E_n matrix gives the initial conditions to be applied at the ith end of shell segment n for the final integration (see step 7 of Fig. 8).

Further Remarks

The use of forward integration for solution of the shell equations eliminates the large computer storage requirements associated with the matrix formulation of finite difference equations. The integration scheme used by the authors is the well-known Runge-Kutta method, modified by incorporating an automatic selection of a variable integration step size. This modification holds the error within specified limits and speeds up the computations. Problems of the size of the pressure vessel run from 10 to 20 min on the IBM 7094 digital computer. As described in Ref. 8, there is a practical limit to the length of shell segment that may be handled by this technique. The limit is realistic; ordinary integrating schemes will permit a maximum segment-length parameter $\Lambda > 3$. For the linear case, the influence coefficients are theoretically symmetric by reciprocity. For applications in the authors' experience, the nonlinear problems have nearly symmetric matrices. The final check is agreement of final results at the segment joints.

The final stress and displacement distributions could be obtained by linearly combining the seven unit solutions in accordance with the results of the stiffness analysis. However, it is more efficient to store only stress resultants and displacements at boundaries and interfaces and then use these as initial values for a final integration. The computed N_φ function is compared with the assumed distribution $\bar{N}_\varphi$. If necessary, the problem is repeated using the new data for $\bar{N}_\varphi$.

References

[1] Kempner, J., "Unified shell theory," Polytechnic Institute of Brooklyn, PIBAL Rept. 566 (March 1960).

[2] Reissner, E., "A new derivation of the equations for the deformation of elastic shells," Am. J. Math. **63**, 177–184 (1941).

[3] Sepetoski, W. K., Pearson, C. E., Dingwell, I. W., and Adkins, A. W., "A digital computer program for the general axially symmetric thin shell problem," J. Appl. Mech. **29**, 655–661 (1962).

[4] Timoshenko, S. and Woinowsky-Krieger, S., *Theory of Plates and Shells* (McGraw-Hill Book Co., Inc., New York, 1959), 2nd ed., pp. 534–535.

[5] Wittrick, W. H., "Interaction between membrane and edge stresses for thin cylinders under axially symmetrical loading," J. Roy. Aeron. Soc. **67**, 172–174 **30**, (1963).

[6] Cline, G. B., "Effect of internal pressure on the influence coefficients of spherical shells," J. Appl. Mech. **30**, 91–97 (1963).

[7] Wei, B. C. F., "Structural analysis of solid propellant rocket casings," ARS Preprint 1590-61 (1961).

[8] Kalnins, A., "Analysis of shells of revolution subjected to symmetrical and nonsymmetrical loads," J. Appl. Mech. **31**, 467–476 (1964).

[9] Cohen, G. A., "Computer analysis of asymmetrical deformation of orthotropic shells of revolution," AIAA J. **2**, 932–934 (1964).

[10] Reissner, E., "On the theory of thin elastic shells," Reissner Anniversary Volume (J. W. Edwards, Ann Arbor, Mich., 1949) pp. 231–247.

[11] Reissner, E., "On axisymmetrical deformations of thin shells of revolution," *Proceeding of the Symposium on Applied Mathematics* (McGraw-Hill Book Company, Inc., New York, 1950), Vol. 3, pp. 27–52.

JULY 1965 AIAA JOURNAL VOL. 3, NO. 7

Uniform-Stress Spinning Filamentary Disk

A. C. KYSER*
Astro Research Corporation, Santa Barbara, Calif.

An analysis is presented for the development of the fiber patterns necessary to produce uniform fiber tension in a spinning filamentary disk. The family of fiber patterns for such isotensoid disks is described in terms of curvature, slope, and arc length, and means are suggested for obtaining polar-coordinate plots of the patterns. Included are diagrams of three of the patterns, a photograph of a model, and a discussion of the general characteristics of the family of allowable patterns. It was found that the isotensoid disk design by which the disk is covered by uniform-diameter fibers operates at half the stress of a simple hoop for a given peripheral velocity and fiber material.

Nomenclature

r = radius coordinate
r_o = radius of disk
R = r/r_o, nondimensional radius coordinate
β = angle between fiber and radius vector
ρ = radius of curvature of fiber
ω = rotation speed of disk
m' = mass per unit length along fiber
Ω = $m'\omega^2 r_o^2/T$, fiber loading parameter
F' = interfiber shear force per unit length
T = tension in structural fiber
θ = angle swept by tangent to fiber
φ = central angle coordinate
l = arc length along fiber, measured from periphery of disk
L = l/r_o, nondimensional arc length
x = R^2, nondimensional radius coordinate
s = stress in structural fiber
γ = weight density of fiber material
λ = s_{ult}/γ, specific strength of fiber
v_o = peripheral velocity of rotating disk

Introduction

THIS paper presents the analytical development of a uniform-stress (isotensoid) spinning disk composed of structural filaments of uniform cross section. The filamentary arrangement is that of a fine-mesh circular net in which the fibers form curved load-carrying paths that spiral outward from the center. It can be shown that any spiral net will carry a radially directed loading in such a way that the resultant fiber tension decreases toward the center of the net. This tension gradient is the result of the spiral load-path curvature. The fiber tension resulting from the inertia forces due to rotation, on the other hand, tends to increase toward the center. The constant-tension condition can be imposed by arranging for the curvature distribution to be that which is necessary to allow these two tension-gradient effects to cancel.

This work may be considered an extension of the work done in Refs. 1 and 2. In Ref. 1, a theory was developed for predicting equilibrium shapes of filamentary structures in which the structural loads are carried in pure tension. This paper was specifically concerned with normal loads on the fiber (i.e., pressure loads), and the solutions were presented in terms of differential equations describing the local curvature and/or slope of the structural wall in terms of the local conditions. In Ref. 2, this problem was generalized to include load components tangential to the structural wall (from centrifugal effects), and solutions for the curvature and slope equations were obtained in the form of elliptic integrals. The present paper represents a further generalization in that allowance is made for an internally generated shear stress in the filamentary wall.

This type of structure is proposed for space applications where requirements exist for large rotating surfaces in which the loads generated by the mass of rotating structure are important. One such application is suggested by Ref. 3, which discusses the use of a lightweight woven fabric net as a low-loading, low-temperature, rotating wing for re-entry deceleration. Other possible applications include the use of filamentary disks to support large surfaces for the collection or reflection of radiant energy. It is believed that an isotensoid disk of this type, in addition to having the excellent mechanical properties characteristic of filamentary structures, can be made to have a high structural efficiency.

Received June 19, 1964; revision received November 16, 1964. The work reported here was conducted with the financial support of NASA.

* Senior Engineer.